Original Article | Experimental and Others

http://dx.doi.org/10.3348/kjr.2014.15.5.591
pISSN 1229-6929 · eISSN 2005-8330
Korean J Radiol 2014;15(5):591-604

Korean Journal of Radiology
KJR

Intratumoral Heterogeneity of Breast Cancer Xenograft Models: Texture Analysis of Diffusion-Weighted MR Imaging

Bo La Yun, MD[1, 2], Nariya Cho, MD[1], Mulan Li, PhD[1], Min Hye Jang, MD[3], So Yeon Park, MD, PhD[3], Ho Chul Kang, PhD[4], Bohyoung Kim, PhD[2], In Chan Song, PhD[1], Woo Kyung Moon, MD[1]

[1]Department of Radiology, Seoul National University Hospital, Seoul National University College of Medicine, Seoul 110-744, Korea; Departments of [2]Radiology and [3]Pathology, Seoul National University Bundang Hospital, Seongnam 463-707, Korea; [4]Department of Computer Science and Engineering, Seoul National University, Seoul 151-744, Korea

Objective: To investigate whether there is a relationship between texture analysis parameters of apparent diffusion coefficient (ADC) maps and histopathologic features of MCF-7 and MDA-MB-231 xenograft models.

Materials and Methods: MCF-7 estradiol (+), MCF-7 estradiol (-), and MDA-MB-231 xenograft models were made with approval of the animal care committee. Twelve tumors of MCF-7 estradiol (+), 9 tumors of MCF-7 estradiol (-), and 6 tumors in MDA-MB-231 were included. Diffusion-weighted MR images were obtained on a 9.4-T system. An analysis of the first and second order texture analysis of ADC maps was performed. The texture analysis parameters and histopathologic features were compared among these groups by the analysis of variance test. Correlations between texture parameters and histopathologic features were analyzed. We also evaluated the intraobserver agreement in assessing the texture parameters.

Results: MCF-7 estradiol (+) showed a higher standard deviation, maximum, skewness, and kurtosis of ADC values than MCF-7 estradiol (-) and MDA-MB-231 ($p < 0.01$ for all). The contrast of the MCF-7 groups was higher than that of the MDA-MB-231 ($p = 0.004$). The correlation (COR) of the texture analysis of MCF-7 groups was lower than that of MDA-MB-231 ($p < 0.001$). The histopathologic analysis showed that Ki-67$_{mean}$ and Ki-67$_{diff}$ of MCF-7 estradiol (+) were higher than that of MCF-7 estradiol (-) or MDA-MB-231 ($p < 0.05$). The microvessel density (MVD)$_{mean}$ and MVD$_{diff}$ of MDA-MB-231 were higher than those of MCF-7 groups ($p < 0.001$). A diffuse-multifocal necrosis was more frequently found in MDA-MB-231 ($p < 0.001$). The proportion of necrosis moderately correlated with the contrast ($r = -0.438$, $p = 0.022$) and strongly with COR ($r = 0.540$, $p = 0.004$). Standard deviation ($r = 0.622$, $r = 0.437$), skewness ($r = 0.404$, $r = 0.484$), and kurtosis ($r = 0.408$, $r = 0.452$) correlated with Ki-67$_{mean}$ and Ki-67$_{diff}$ ($p < 0.05$ for all). COR moderately correlated with Ki-67$_{diff}$ ($r = -0.388$, $p = 0.045$). Skewness ($r = -0.643$, $r = -0.464$), kurtosis ($r = -0.581$, $r = -0.389$), contrast ($r = -0.473$, $r = -0.549$) and COR ($r = 0.588$, $r = 0.580$) correlated with MVD$_{mean}$ and MVD$_{diff}$ ($p < 0.05$ for all).

Conclusion: The texture analysis of ADC maps may help to determine the intratumoral spatial heterogeneity of necrosis patterns, amount of cellular proliferation and the vascularity in MCF-7 and MDA-MB-231 xenograft breast cancer models.

Index terms: *Animal; Breast neoplasms; Diffusion magnetic resonance imaging; Image interpretation; Computer-assisted*

Received March 20 2014; accepted after revision June 7, 2014.
This research was supported by Basic Science Research Program through the National Research Foundation of Korea (NRF) funded by the Ministry of Education, Science and Technology (2012R1A1A1006722), and by a grant (no. 04-2012-0270) from the Seoul National University Hospital Research Fund.

Corresponding author: Nariya Cho, MD, Department of Radiology, Seoul National University Hospital, Seoul National University College of Medicine, 101 Daehak-ro, Jongno-gu, Seoul 110-744, Korea.
• Tel: (822) 2072-1861 • Fax: (822) 743-6385 • E-mail: river7774@gmail.com

INTRODUCTION

It has been well established that breast cancer is a heterogeneous disease. The gene expression profiling analysis resulted in the classification of several breast cancer subtypes (luminal A, luminal B, human epidermal growth factor receptor2-positive and triple-negative), showing various prognosis and therapeutic outcomes (1). Systemic treatment recommendations follow the subtype classification and current approaches to molecular biomarker testing focus on this inter-patient tumor heterogeneity. However, as predictive biomarkers evolve during tumor progression or treatment, the intratumoral heterogeneity is also believed to be related to clinical outcomes (2). Several ongoing clinical trials are using multiregional samplings to evaluate the intratumoral heterogeneity and evolution in relation to the drug treatment. However, the genomic assessment of intratumoral heterogeneity has many practical challenges for its clinical application, including imprecision in the spatial orientation of tumor sample blocks or sampling bias from data obtained in a limited geographical region. It would be ideal to develop non-invasive imaging techniques for the characterization or monitoring of intratumoral heterogeneity.

Diffusion-weighted magnetic resonance imaging (DW-MRI) with apparent diffusion coefficient (ADC) has been increasingly used in the field of oncology. Signals from DW-MRI originate from restrictions to the random movement of water between cell membranes of tissues, which reflects tumor cellularity and the integrity of cell membranes (3). The quick imaging without the need for an exogenous contrast medium allows the clinical application of DW-MRI with ADC to expand from the differentiation of benign and malignant tumors, the screening of cancers and the monitoring of the response to chemotherapeutic treatment to prognostic applications (4-9). Recently, a study using the xenograft tumor model found that ADC values of the solid portion of tumors correlated with intratumoral necrosis and microvessel density in prostate cancers (10). Additionally, distributions of ADC values have correlated with tumor growth rates and the expression of Ki-67, hypoxia inducible factor 1 alpha (HIF-1α), and vascular endothelial growth factor receptor (VEGFR)-2 in breast cancers (11).

The texture analysis, which relies on mathematical methods to describe relationships between the grey level of pixels and their spatial information, has been emerging in the field of medical imaging for the purpose of establishing a quantification technique for spatial heterogeneity (12, 13). Grey level co-occurrence matrix (GLCM) is one of the most frequently used texture analysis methods in the field of medical imaging. The GLCM analysis calculates the relative frequency matrix generated by counting the occurrences of intensity pairs between the current and neighboring pixels in a given grey-level image (14). So, a better tissue characterization and prediction of therapy response and survival has been applied in contrast-enhanced MRI and ^{18}F-fluorodeoxyglucose positron emission tomography scans through the evaluation of the inter-relationship of the pixels (15-22). However, few studies have reported its application to the evaluation of the intratumoral heterogeneity of various breast cancer xenograft model subtypes as characterized by DW-MRI.

Thus, the purpose of this study was to determine whether there is a relationship between texture analysis parameters of the ADC maps and histopathologic features of MCF-7 and MDA-MB-231 xenograft models.

MATERIALS AND METHODS

This study was approved by the Institutional Animal Care and Use Committee of the Seoul National University Hospital Biomedical Research Institute and was performed under the guidelines of the National Institutes of Health for the care and use of laboratory animals.

MCF-7 and MDA-MB-231 Tumor Models

MCF-7 and MDA-MB-231 cell lines (American Type Culture Collection, Manassas, VA, USA) were cultured and prepared for the inoculation in an orthotropic xenograft model. Twenty-one female nonobese diabetic-severe combined immunodeficient mice, aged six weeks (Orient, Seoul, Korea), received subcutaneous injections of approximately 5 x 10^6 cells (in 50 μL serum free media) mixed with 50 μL Matrigel (BD Biosciences, Franklin Lakes, NJ, USA) into bilateral abdominal mammary fat pads. Fourteen mice were pre-treated for the MCF-7 groups with 3 mg/kg of beta-estradiol 17-cypionate (Sigma-Aldrich, St. Louis, MO, USA) by subcutaneous injection, starting two weeks before the cell implantation. The pre-treated mice were then divided into two groups: MCF-7 estradiol (+) and MCF-7 estradiol (-). The MCF-7 estradiol (+) group received an additional weekly estradiol injection until the MR imaging. No additional estradiol supplement was given after cell implantation to the MCF-7 estradiol (-) group. Seven mice were implanted

Korean Journal of Radiology
KJR

with the MDA-MB-231 cell line and did not receive estradiol supplement. MR images were acquired when the maximal diameter of the tumor had reached 10 mm.

DW-MRI and Texture Analysis

Diffusion-weighted magnetic resonance imaging was performed with a 9.4-T MR imaging system (Varian, Magnex Scientific Ltd., Palo Alto, CA, USA) equipped with a surface coil. The animals were anesthetized with isoflurane (1–2% in 100% oxygen) during MR imaging. Body temperature and respiratory rate were continuously monitored using pressure-sensitive and rectal temperature probes. An air warmer was used to maintain the body temperature throughout the experiments. The MR imaging protocol included the following sequences: 1) a sagittal T2-weighted fast spin-echo sequence (FSE) (repetition time/echo time, 3000 msec/25 msec; matrix, 128 x 96; field of view, 30 x 20 mm; section thickness, 1 mm; gap, 1 mm), 2) axial diffusion-weighted images obtained by FSE (repetition time/echo time, 3000 msec/27 msec; average, 2; echo train length, 4; matrix, 96 x 128; field of view, 20 x 30 mm; section thickness, 1 mm; gap, 0–0.2 mm) with eight b factors (b = 0, 50, 100, 150, 200, 400, 600, and 800 sec/mm^2) in three orthogonal gradient directions (x, y, and z). Bilateral implanted tumors were imaged together.

The image analysis was performed by an experienced radiologist (8 years of experiences in imaging analysis). The tumor volume was calculated in sagittal T2-weighted FSE images and axial DW-FSE (b = 0) images by the equation: volume = 3.14 x height x width x length ÷ 6. The ADC, based on the Stejskal and Tanner (23) equation, was calculated using the linear regression algorithm for best fitting the points for b versus ln (SI), where SI is the signal intensity from a region of interest (ROI) of the images acquired at the eight b values. A home-made software package to obtain ADC maps on a pixel-by-pixel basis was developed in an IDL platform (ITT Visual Information Solutions, Boulder, CO, USA). ROIs were drawn along the outline of the tumor in the ADC image showing the largest tumor diameter. The mean, standard deviation, quartiles, minimum, maximum, skewness and kurtosis of the ADC values were calculated for the first order texture analysis. The second order texture analysis (GLCM) was used to evaluate the spatial relationship of the pixels. Of several calculated features derived from GLCM, we used five features related with regional heterogeneity which were frequently used in previous studies (12). Contrast, entropy, homogeneity, uniformity and correlation (COR) of the ADC values within the ROI were calculated using in-house GLCM software as follows (24):

$$\text{Contrast} = \sum_{n=0}^{N-1} n^2 \left\{ \sum_{i=1}^{N} \sum_{j=1}^{N} p(i,j) \right\}, |i-j| = n$$

$$\text{Entropy} = -\sum_{i=0}^{N-1} \sum_{j=0}^{N-1} p(i,j) \log\left(p(i,j)\right)$$

$$\text{Homogeneity} = \sum_{i=0}^{N-1} \sum_{j=0}^{N-1} \frac{p(i,j)}{1+(i-j)^2}$$

$$\text{Uniformity} = \sum_{i=0}^{N-1} \sum_{j=0}^{N-1} \{p(i,j)\}^2$$

$$\text{Correlation (COR)} = \sum_{i=0}^{N-1} \sum_{j=0}^{N-1} \frac{(ij)p(i,j) - \mu_x \mu_y}{\sigma_x \sigma_y}$$

The variables i and j represent the grey values in the ADC map, p (i, j) is the (i, j)th entry in a normalized GLCM and N is the number of distinct grey levels in an image. The variables μ_x and μ_y are means of p_x and p_y and variables σ_x and σ_y are standard deviations of p_x and p_y.

To evaluate the intraobserver variability, the same radiologist measured the same parameters 4 months later.

Quantification of Histopathologic Features

Immediately after MR image acquisition, all mice were euthanized with CO_2 narcosis followed by a thoracotomy. The tumors were excised with overlying skin. The cephalic direction of the skin was marked. Paraffin-embedded tissues were cut into 5-μm thick sections in the plane parallel to the axial MR image. Two pathologists, both blinded to the tumor cell type, performed all pathologic examinations. Hematoxylin and eosin staining was performed for the analysis of the distribution and amount of necrosis. The proportion of necrosis within the tumor was quantified. The distribution of necrosis was classified as a central and diffuse multifocal pattern.

An immunohistochemical staining of the proliferation marker, Ki-67 was conducted, using a rabbit monoclonal antibody (Abcam, Cambridge, UK; Clone SP6, dilution 1:100). The Ki-67 antibody-stained slides were scanned using an AperioScanScope (Aperio Technologies, Vista, CA, USA) with a nuclear algorithm. The areas of highest and lowest density of Ki-67-positive cells were selected. The Ki-67 index was calculated by the fraction of Ki-67 positive cells on samples of at least 500 tumor cells. The mean Ki-67

index for the lowest and highest density area is labeled Ki-67_{mean}. The difference in the Ki-67 index between the lowest and highest density areas is represented by Ki-67_{diff}. The pan-endothelial marker, CD34, was stained using a rabbit monoclonal antibody (Abcam, Cambridge, UK; Clone EP373Y, dilution 1:100) for microvessel staining. The lowest and highest vascular areas were selected on low power fields (x 40) and the microvessel density (MVD) was calculated when CD34-positive endothelial or clustered cells were present under high power field (x 200) examination. The mean MVD in the highest and the lowest vascular areas are denoted as MVD_{mean}. The MVD difference between the lowest and highest vascular areas are denoted as MVD_{diff}.

Exclusions

Of the 21 mice, two mice (including one MCF-7 estradiol (-) and one MDA-MB 231) were excluded due to unwanted death during MR examinations. To minimize the effect of tumor volume on heterogeneity, we only included tumors with a volume in the range of 500 to 1500 mm^3, because larger tumors tend to have a higher hypoxic fraction and necrosis (25). Finally, 12 tumors of the MCF-7 estradiol (+) group, 9 tumors of the MCF-7 estradiol (-) group and 6 tumors of the MDA-MB-231 group were included for the analysis.

Data and Statistical Analysis

Statistical analyses were performed using PASW statistics version 18 (IBM SPSS, Chicago, IL, USA) and MedCalc 10.0.0.0 (MedCalc Software, Ostend, Belgium). A normal distribution was verified by the Kolmogorov-Smirnov test.

The first and second order texture analysis parameters were compared among the three groups using the analysis of variance test or the Kruskal-Wallis test. A post-hoc analysis using Bonferroni method was performed if the results were significant. The Fisher's exact test was performed for the comparison of the necrosis patterns. Then, we performed a correlation analysis between the texture analysis parameters from DW-MRI and histopathologic features using the Pearson correlation test. The intraobserver variability of ROI measurement was evaluated by using intraclass correlation coefficients (ICCs) with a two-way mixed consistency model. When the p value was less than 0.05, the results were considered significant.

RESULTS

No difference was found in tumor volumes among the MCF-7 estradiol (+) group, MCF-7 estradiol (-) group, and MDA-MB-231 group (mean ± standard deviation, 808.1 ± 143.9 mm^3, 757.1 ± 142.7 mm^3, and 944.9 ± 341.7 mm^3, p = 0.221, respectively) (Fig. 1A).

Texture Parameters

The MCF-7 estradiol (+) group, showed a significantly higher standard deviation (398 x 10^{-6} mm^2/sec, 235 x 10^{-6} mm^2/sec, and 213 x 10^{-6} mm^2/sec, respectively; p < 0.001), a higher maximum value (2610 x 10^{-6} mm^2/sec, 1904 x 10^{-6} mm^2/sec, and 2149 x 10^{-6} mm^2/sec, respectively; p < 0.001), a higher skewness (2.7, 1.8, and 1.2, respectively; p < 0.001), and a higher kurtosis (7.3, 4.7, and 3.5, respectively; p = 0.001) as compared with the MCF-7 estradiol (-) or MDA-MB-231 groups. A higher standard deviation indicates much dispersion of the value distribution from the mean. A higher kurtosis indicates a sharp peak and/or wide tail of the value distribution. A higher positive skewness means more asymmetry from the normal distribution plot. Our results showed a more heterogeneous intratumoral ADC pixel value in the MCF-7 estradiol (+) group (Table 1, Fig. 1). With regard to the second order texture GLCM analysis, the contrast of the MCF-7 estradiol (+) or estradiol (-) groups was significantly higher than that of the MDA-MB-231 group (476, 536, and 288, respectively; p = 0.004), and the COR of the MCF-7 estradiol (+) group and estradiol (-) group were significantly lower than that of the MDA-MB-231 group (0.4 x 10^{-3}, 0.8 x 10^{-3}, and 2.0 x 10^{-3}, respectively; p < 0.001) (Table 1, Fig. 2). The contrast measures the local variations in signal intensity between a pixel and a neighbor pixel. The COR measures a joint probability occurrence between a pixel and a neighbor pixel in a whole region. Our results showed that the MCF-7 groups had more various signal intensities between neighboring pixel pairs than MDA-MB-231 group and had less joint probability occurrences between neighboring pixel pairs.

On the texture analysis, there was no difference in the mean, median, first and third quintile ADC value, entropy, homogeneity and uniformity among the three groups. The ICCs between two repeated measurements of texture parameters were more than 0.85 in all parameters, but of minimum value (Table 2).

Histopathologic Features

The proportion of necrosis in the MCF-7 estradiol (+) and (-) groups was lower than that in the MDA-MB-231 group

Korean Journal of Radiology
KJR

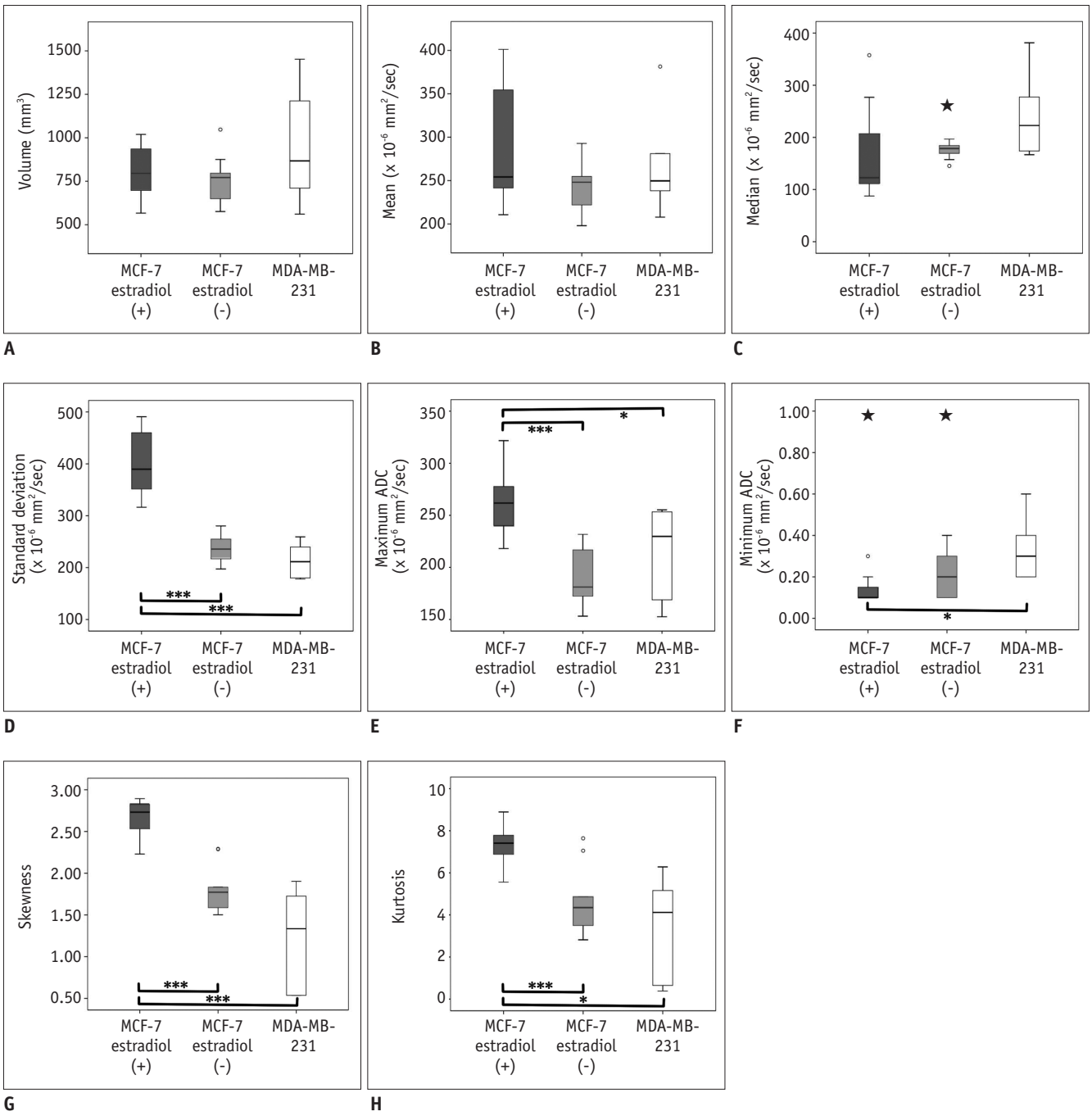

Fig. 1. Box-and-whisker plot of volumes and first order texture analysis parameters of tumor groups.
(A) Volume, **(B)** mean, **(C)** median, **(D)** standard deviation, **(E)** maximum, **(F)** minimum, **(G)** skewness, and **(H)** kurtosis of ADC maps for MCF-7 estradiol (+) (dark grey boxes), MCF-7 estradiol (-) (light grey boxes) and MDA-MB-231 (white boxes) groups. *Statistical significance with $p < 0.05$, **Statistical significance with $p < 0.01$, ***Statistical significance with $p < 0.001$. ○: observations 1.5 interquartile ranges (IQRs) from end of box, ★: observations 3 IQRs from end of box. ADC = apparent diffusion coefficient

(23.8%, 18.3%, and 35.8%, respectively; $p = 0.008$). A central pattern necrosis was found in both MCF-7 groups but not in the MDA-MB-231 group, whereas a diffuse multifocal pattern necrosis was more frequently found in the MDA-MB-231 group ($p < 0.001$). With regard to Ki-67, the MCF-7 estradiol (+) group showed the highest $Ki\text{-}67_{mean}$ value followed by the MDA-MB-231 group and the MCF-7 estradiol (-) group. $Ki\text{-}67_{diff}$ was higher in the MCF-7 estradiol (+) group than in the MDA-MB-231 or MCF-7 estradiol (-) groups. The MDA-MB-231 group showed a higher MVD_{mean} and MVD_{diff} than the MCF-7 estradiol (+) or estradiol (-) groups (Table 3, Fig. 3).

Table 1. Comparison of Texture Parameters of ADC Map among MCF-7 Estradiol (+), MCF-7 Estradiol (-), and MDA-MB-231 Groups

	MCF-7 Estradiol (+) (Mean ± SD) (n = 12)	MCF-7 Estradiol (-) (Mean ± SD) (n = 9)	MDA-MB-231 (Mean ± SD) (n = 6)	*P*
First order texture				
Mean*	287 ± 70	243 ± 29	268 ± 60	0.474
First quartile*	64 ± 48	66 ± 23	89 ± 42	0.100
Second quartile (median)*	163 ± 84	183 ± 34	241 ± 82	0.051
Third quartile*	308 ± 97	337 ± 36	388 ± 85	0.111
Standard deviation*	398 ± 61	235 ± 29	213 ± 33	< 0.001
Minimum value*	0.2 ± 0.3	0.3 ± 0.3	0.3 ± 0.2	0.025
Maximum value*	2610 ± 290	1904 ± 275	2149 ± 440	< 0.001
Skewness	2.7 ± 0.2	1.8 ± 0.3	1.2 ± 0.6	< 0.001
Kurtosis	7.3 ± 0.9	4.7 ± 1.6	3.5 ± 2.4	0.001
Second order texture				
Contrast	476 ± 104	536 ± 147	288 ± 143	0.004
Entropy	6.4 ± 1.5	6.6 ± 1.5	6.8 ± 0.7	0.839
Homogeneity	0.3 ± 0.2	0.2 ± 0.2	0.2 ± 0.1	0.577
Uniformity	0.06 ± 0.10	0.05 ± 0.09	0.01 ± 0.02	0.787
Correlation†	0.4 ± 0.2	0.8 ± 0.2	2.0 ± 1.2	< 0.001

Note.— *Unit: x 10^{-6} mm^2/sec, †Unit: x 10^{-3}. ADC = apparent diffusion coefficient, SD = standard deviation

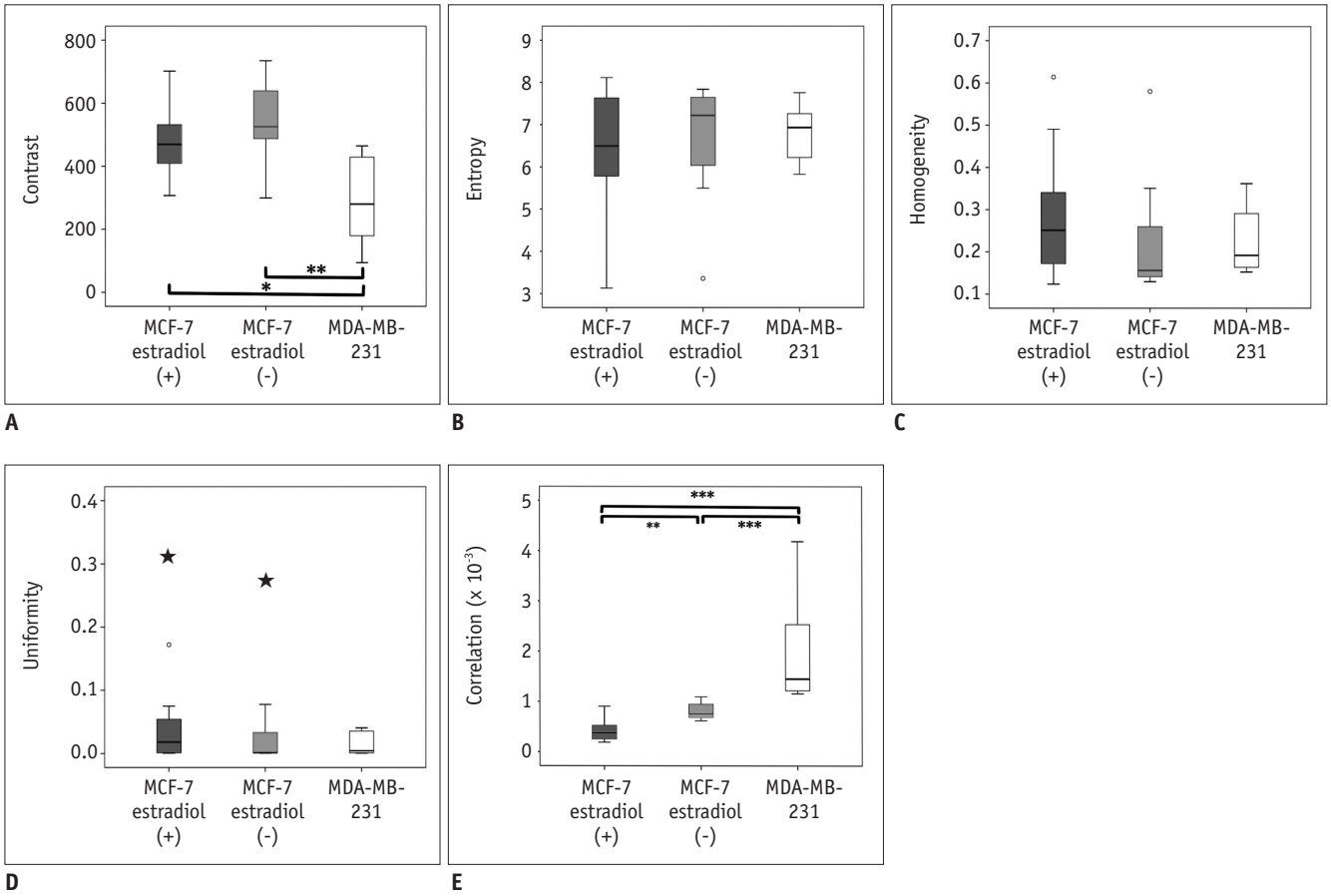

Fig. 2. Box-and-whisker plot of second order texture analysis parameters of tumor groups.
(A) Contrast, **(B)** entropy, **(C)** homogeneity, **(D)** uniformity, and **(E)** correlation of ADC maps are shown for MCF-7 estradiol (+) (dark grey boxes), MCF-7 estradiol (-) (light grey boxes), and MDA-MB-231 (white boxes) groups. *Statistical significance with $p < 0.05$, **Statistical significance with $p < 0.01$, ***Statistical significance with $p < 0.001$. ○: observations 1.5 interquartile ranges (IQRs) from end of box, ★: observations 3 IQRs from end of box. ADC = apparent diffusion coefficient

Korean Journal of Radiology
KJR

Relationship between Texture Parameters and Histopathologic Features

The representative cases showed the relationship between ADC maps and histopathologic results (Fig. 4). The proportion of necrosis inversely correlated moderately with contrast (r = -0.438, p = 0.022) and strongly correlated with COR (r = 0.540, p = 0.004). Ki-67$_{mean}$ and Ki-67$_{diff}$ correlated with the standard deviation (r = 0.622, p = 0.001 and r = 0.437, p = 0.023), skewness (r = 0.404, p = 0.036 and r = 0.484, p = 0.011), and kurtosis (r = 0.408, p = 0.035 and r = 0.452, p = 0.018) of the ADC values. And the COR inversely correlated moderately with Ki-67$_{diff}$ (r = -0.388, p = 0.045) (Fig. 5). MVD$_{mean}$ and MVD$_{diff}$ inversely correlated with the skewness (r = -0.643, p < 0.001 and r = -0.464, p = 0.015), kurtosis (r = -0.581, p = 0.001 and r = -0.389, p = 0.045) and contrast (r = -0.473, p = 0.013 and r = -0.549, p = 0.003) of the ADC maps. MVD$_{mean}$ and MVD$_{diff}$ correlated with COR (r = 0.588, p = 0.001; r = 0.580, p = 0.002) (Fig. 6).

Table 2. Intraobserver Agreement for Measurement of Texture Parameters

	Intraclass Correlation Coefficients	95% CI
First order texture		
Mean	0.98	0.96–0.99
Second quartile (median)	0.97	0.94–0.99
Standard deviation	0.99	0.98–1.00
Minimum value	0.27	-0.12–0.59
Maximum value	0.89	0.76–0.95
Skewness	0.96	0.90–0.98
Kurtosis	0.94	0.86–0.97
Second order texture		
Contrast	0.99	0.98–1.00
Entropy	1.00	0.99–1.00
Homogeneity	1.00	1.00–1.00
Uniformity	1.00	1.00–1.00
Correlation	0.99	0.99–1.00

Note.— CI = confidence interval

DISCUSSION

In our study, the ADC map of the MCF-7 xenograft model with exogenous estradiol supplementation showed more heterogeneous texture parameters, central necrosis and higher Ki-67 values, whereas MDA-MB-231 showed less heterogeneous texture parameters, diffuse multifocal necrosis and higher MVD. The standard deviation, skewness and kurtosis of the ADC map correlated with Ki-67$_{mean}$ and Ki-67$_{diff}$, whereas the COR of the ADC map inversely correlated with Ki-67$_{diff}$. In addition, skewness, kurtosis and contrast inversely correlated with MVD$_{mean}$ and MVD$_{diff}$, whereas the COR correlated with MVD$_{mean}$ and MVD$_{diff}$.

Our results are consistent with those of a previous study, in which triple negative breast cancer xenograft models showed a correlation between the distributions of the ADC value in DW-MRI and tumor growth rates or the expression of Ki-67, HIF-1α, and VEGFR-2 (11). However, these authors did not investigate the differences between the estrogen receptor (ER) (+) and ER (-) subtypes of breast cancer models. In our study, MCF-7 cell lines represented ER (+) breast cancer and MDA-MB-231 cell lines represented the triple negative breast cancer subtype. Compared to the MCF-7 estradiol (-) or MDA-MB-231 tumors, the MCF-7 estradiol (+) tumors showed a higher Ki-67$_{mean}$, indicating a higher cell proliferation. The increased proliferation of ER (+) breast tumors relative to ER (-) MDA-MB-231 tumors can be explained by the mitogenic effect of estradiol, which has been well established (26, 27). The histogram (first

Table 3. Comparison of Histopathologic Features among MCF-7 Estradiol (+), MCF-7 Estradiol (-), and MDA-MB-231 Groups

	MCF-7 Estradiol (+) (Mean ± SD) (n = 12)	MCF-7 Estradiol (-) (Mean ± SD) (n = 9)	MDA-MB-231 (Mean ± SD) (n = 6)	*P*
Proportion of necrosis (%)	23.8 ± 9.3	18.3 ± 5.0	35.8 ± 15.0	0.008
Pattern of necrosis (number, %)				
Central	10 (83)	8 (89)	0 (0)	< 0.001
Diffuse multifocal	2 (17)	1 (11)	6 (100)	
Ki-67 (%)				
Ki-67 mean	52.1 ± 4.6	18.9 ± 5.1	45.1 ± 5.2	< 0.001
Ki-67 difference (highest-lowest)	44.3 ± 13.5	29.8 ± 10.0	26.5 ± 13.4	0.010
Microvessel density (MVD)				
MVD mean*	18 ± 9	18 ± 6	44 ± 11	< 0.001
MVD difference (highest-lowest)*	22 ± 12	11 ± 6	51 ± 17	< 0.001

Note.— *Unit: /high power field. SD = standard deviation

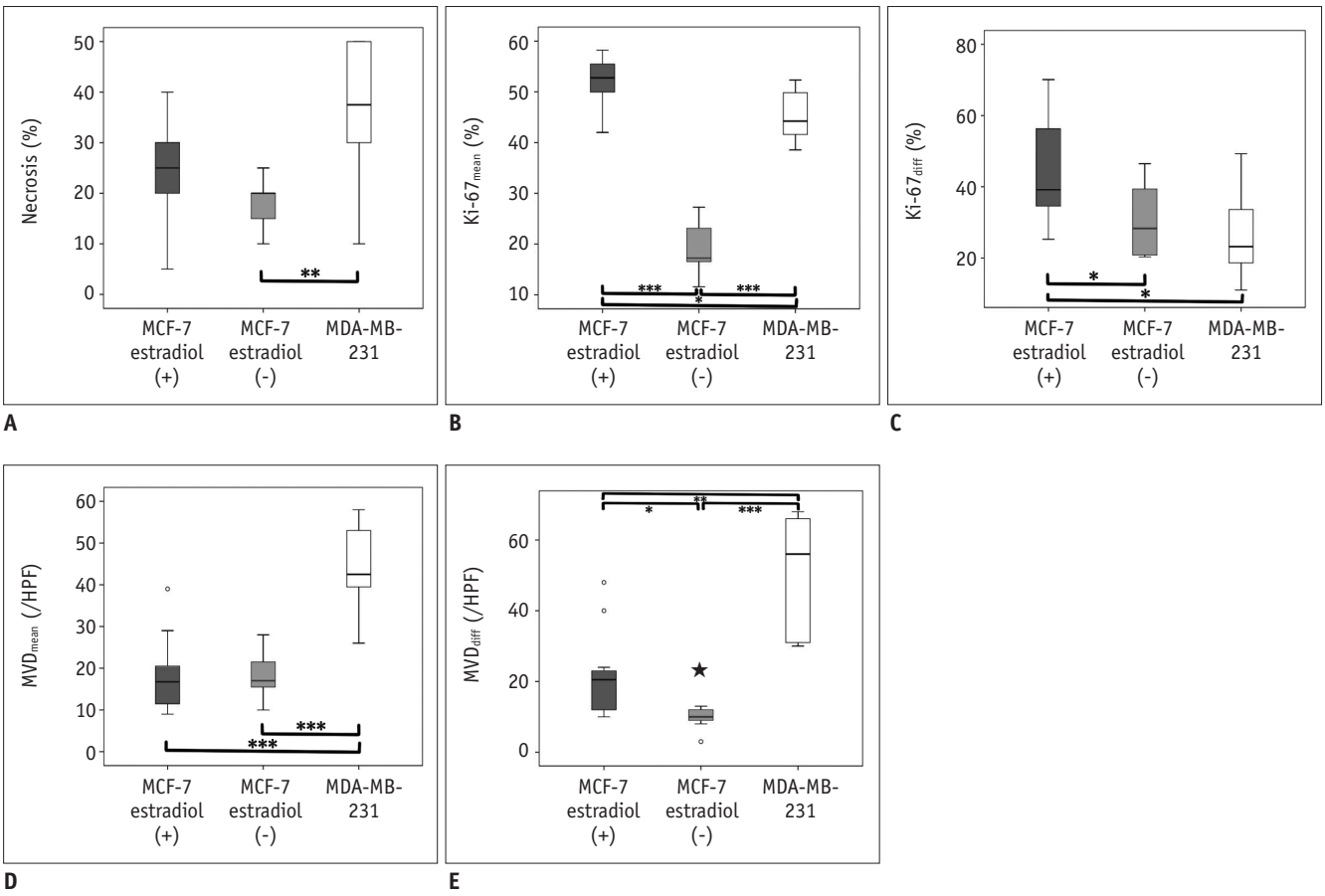

Fig. 3. Box-and-whisker plot of histopathologic features of tumor groups.
(A) Proportion of necrosis, **(B)** Ki-67_{mean}, **(C)** Ki-67_{diff} (highest-lowest), **(D)** MVD_{mean}, and **(E)** MVD_{diff} (highest-lowest) for MCF-7 estradiol (+) (dark grey boxes), MCF-7 estradiol (-) (light grey boxes), and MDA-MB-231 (white boxes) groups are shown. *Statistical significance with $p < 0.05$, **Statistical significance with $p < 0.01$, ***Statistical significance with $p < 0.001$. ○: observations 1.5 interquartile ranges (IQRs) from end of box, ★: observations 3 IQRs from end of box. HPF = high power field, MVD = microvessel density

order texture) analysis of the MCF-7 estradiol (+) ADC map showed a higher standard deviation, a higher skewness (asymmetry of pixel distribution) and a higher kurtosis (peakness of pixel distribution) than the MDA-MB-231 ADC map, suggesting a wider distribution, a higher asymmetry or a sharper ADC distribution peak, which, in general, indicates a greater heterogeneity of ADC histogram (28, 29). Furthermore, Pearson correlation analysis also revealed a positive correlation between these first order texture parameters and higher Ki-67_{mean} and Ki-67_{diff} values.

The second order texture analysis using GLCM is necessary for the assessment of the intratumoral heterogeneity as the grey scale histogram analysis inherently lacks the spatial information of parameters reflecting the distribution of cellularity or necrosis (30). Compared to the MCF-7-derived tumors with or without exogenous estradiol supplementation, the MDA-MB-231-derived tumors showed a low contrast, a high COR in the GLCM analysis, a diffuse multifocal necrosis pattern and a higher MVD_{mean} at histopathology. Moreover, Pearson correlation analysis showed that MVD_{mean} and MVD_{diff} inversely correlated with the skewness, kurtosis and contrast of the ADC values. Additionally, MVD_{mean} and MVD_{diff} correlated with COR. Therefore, we can infer that a lower contrast or a lower difference between neighboring pixel values indicates a lower spatial heterogeneity, which is affected by the vascularity of the tumor. The COR indicates the linearity of the neighboring pixel values. Considering the schematic drawing of Figure 7, even though the three matrices have the same mean and standard deviation with two grey levels, the mosaic pattern shows the lowest COR (-0.09) and the largest area of the same value pattern shows the highest COR (0.75). The large area of similar pixel values leads to a higher COR; the COR value is 1 when all values in the matrix are the same. Thus, the higher COR of the MDA-MB-231 compared to the MCF-7 estradiol (+) group or

Korean Journal of Radiology
KJR

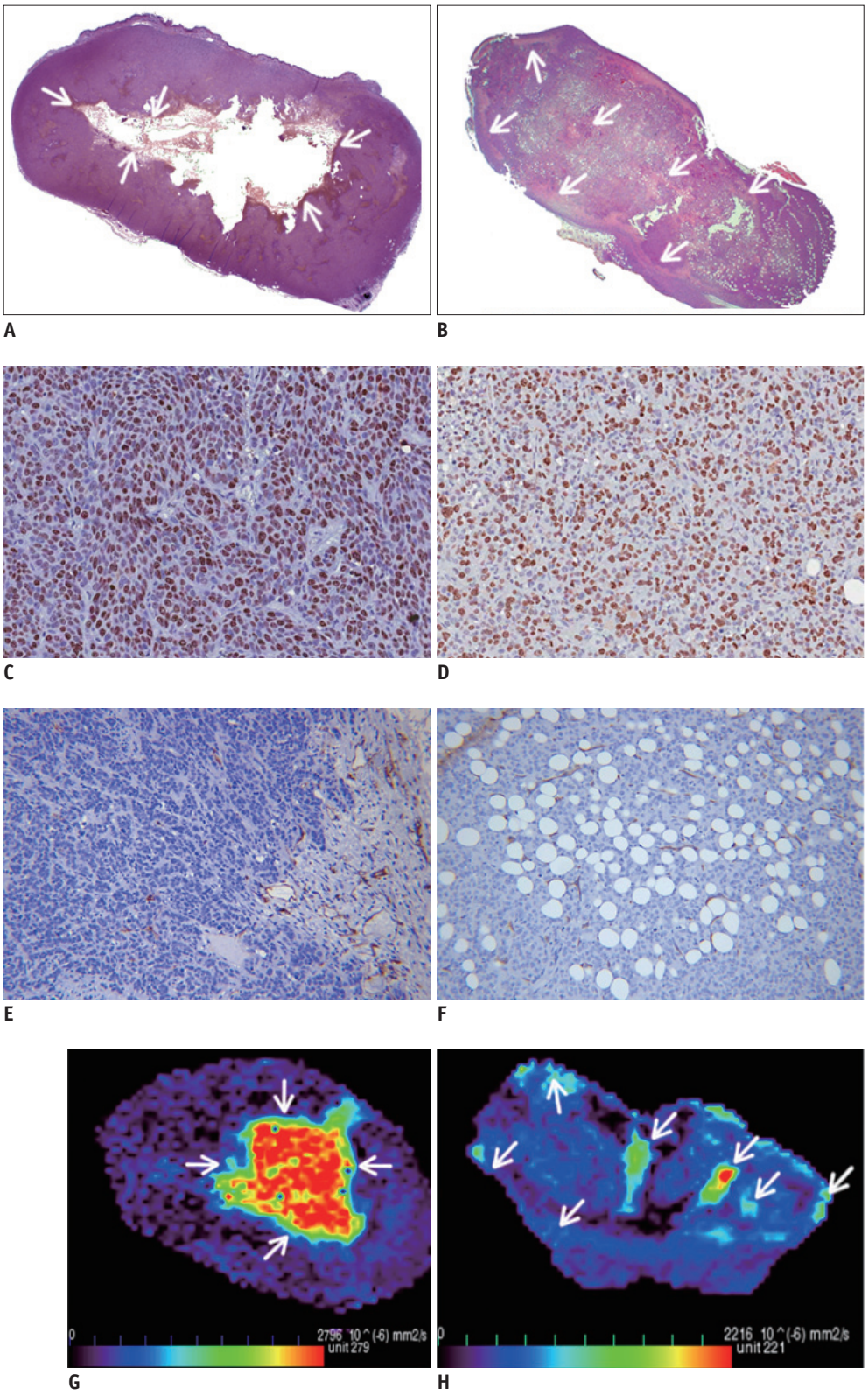

Fig. 4. Relationship between ADC maps and histopathological results.
Photomicrographs of entire section show **(A)** central necrosis (arrows) in MCF-7 estradiol (+) tumor and **(B)** diffuse multifocal necrosis (arrows) in MDA-MB-231 tumor (H&E, x 1.25). Photomicrographs of immunohistochemical staining show high Ki-67 expression in MCF-7 estradiol (+) tumors **(C)** and MDA-MB-231 tumors (x 200) **(D)**. Photomicrographs of immunohistochemical staining for CD34 show low microvessel density in MCF-7 estradiol (+) tumors **(E)** and high microvessel density in MDA-MB-231 tumors (x 200) **(F)**. ADC map **(G)** shows high ADC values in central necrotic portion (arrows) and **(H)** spotty high ADC values (arrows) corresponding to necrosis. ADC = apparent diffusion coefficient, H&E = hematoxylin and eosin

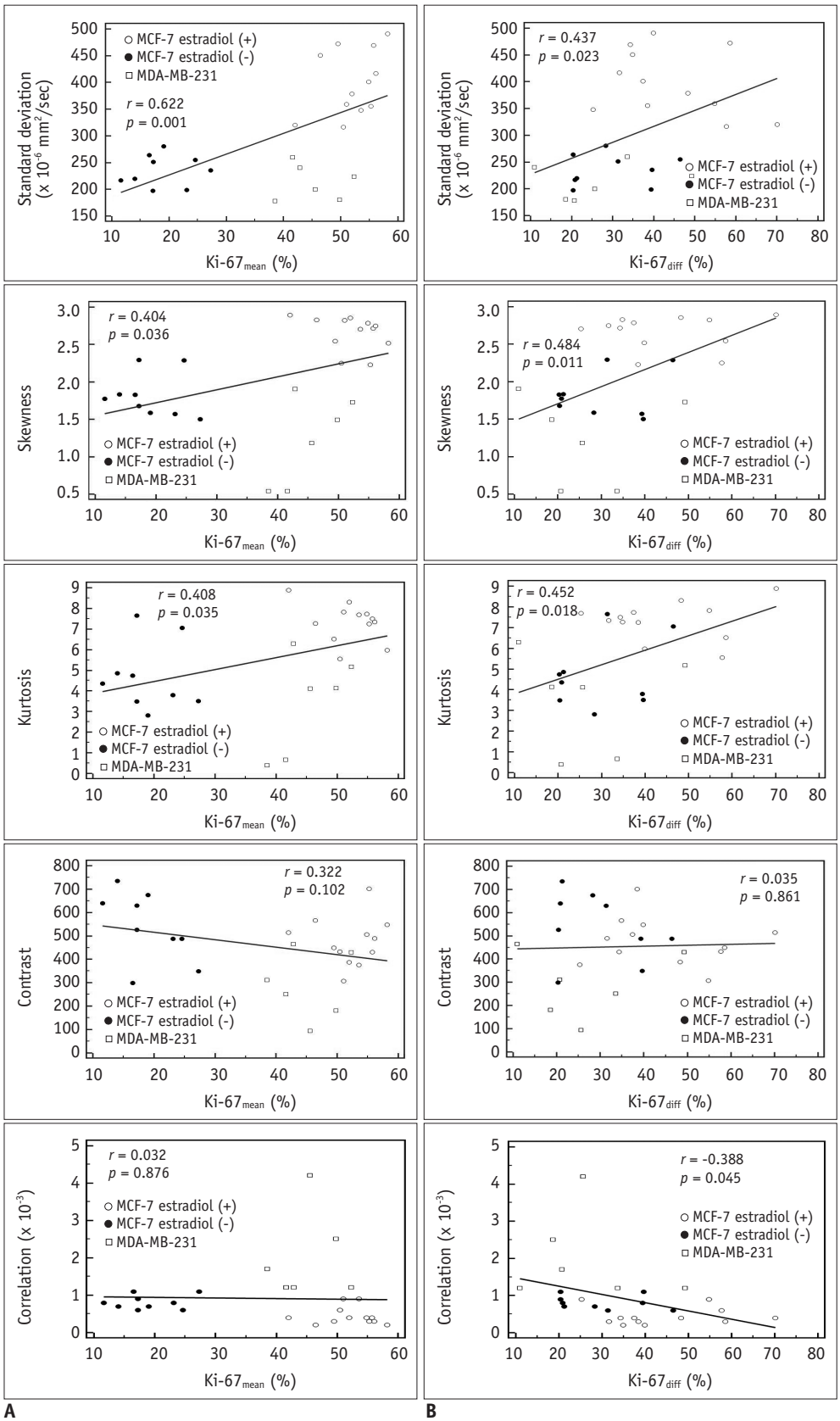

Fig. 5. Relationship between texture parameters and Ki-67 index of tumor groups.
(A) Ki-67$_{mean}$ and **(B)** Ki-67$_{diff}$ showed positive correlation with standard deviation, skewness and kurtosis of ADC texture parameters. However, COR of ADC map showed inverse correlation with Ki-67$_{diff}$. ADC = apparent diffusion coefficient, COR = correlation

Korean Journal of Radiology
KJR

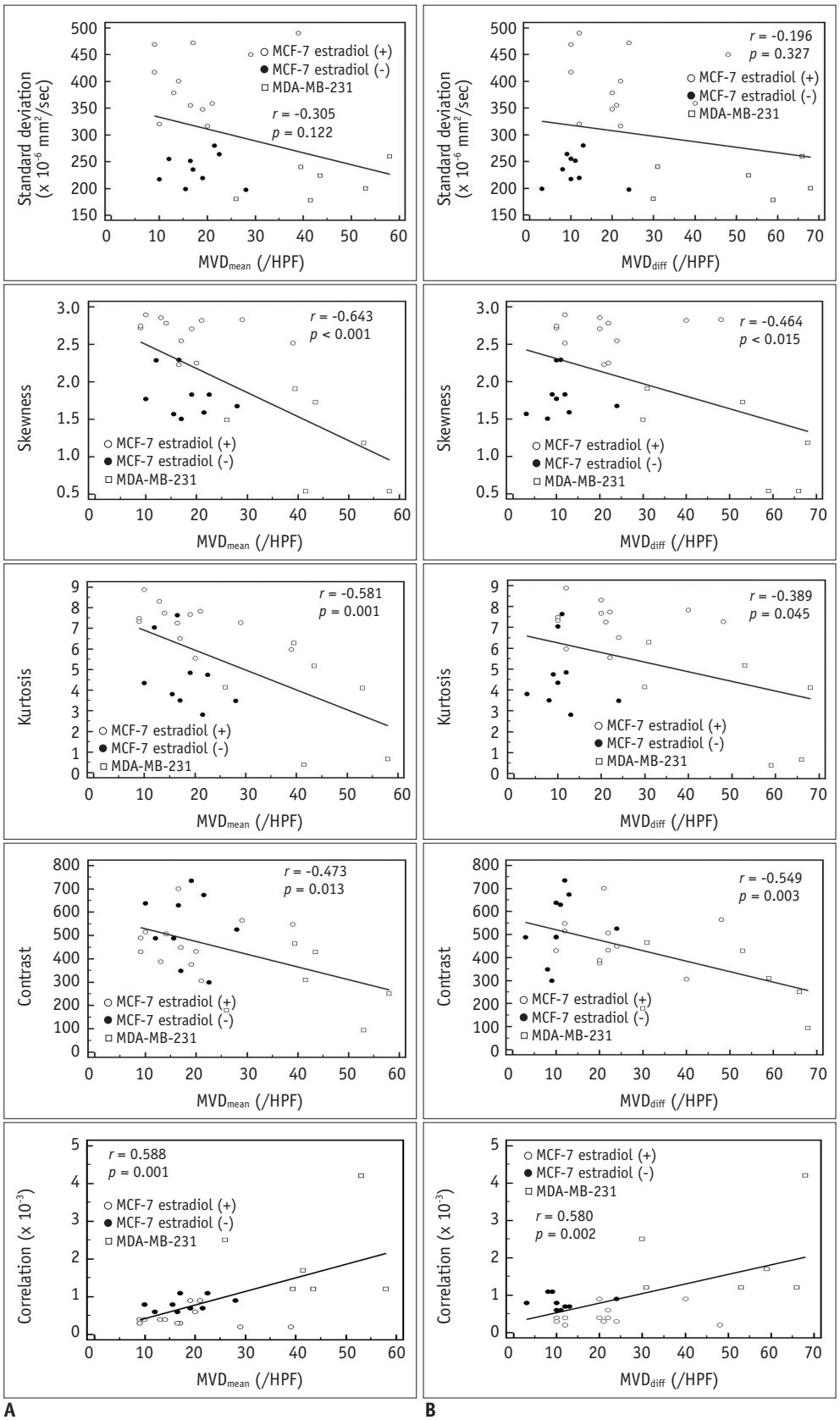

Fig. 6. Relationship between texture parameters and MVD of tumor groups.
(A) MVD_{mean} and **(B)** MVD_{diff} showed inverse correlation with skewness, kurtosis and contrast. COR of ADC map correlated with MVD_{mean} and MVD_{diff}. ADC = apparent diffusion coefficient, COR = correlation, HPF = high power field, MVD = microvessel density

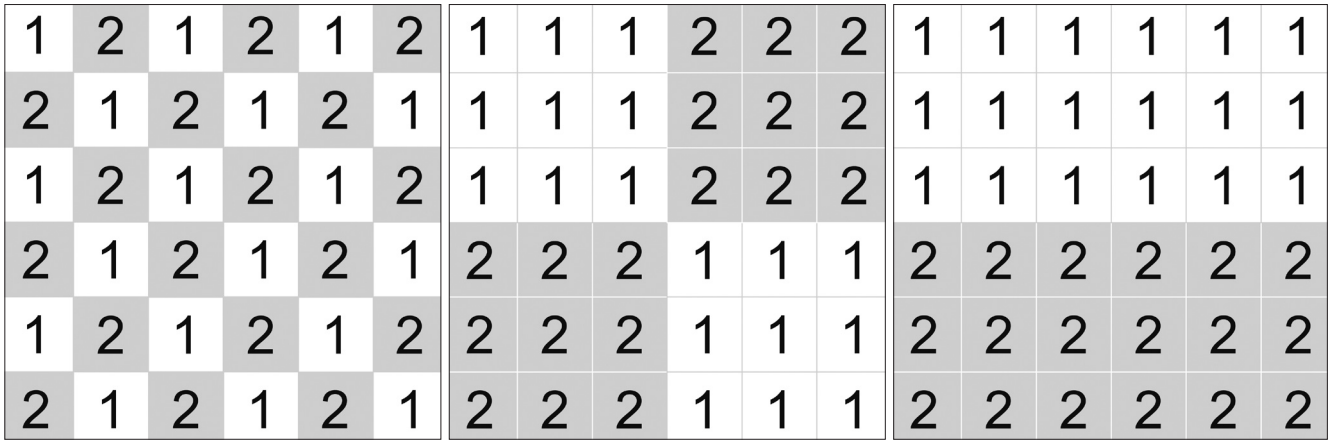

Fig. 7. Three simulations of different correlations.
First-order texture parameters are identical for three cases with mean = 1.5 and standard deviation = 0.5 in all matrices. However, second-order texture parameters derived from grey level co-occurrence matrix varied. **A.** Most heterogeneous mosaic pattern matrix shows lowest correlation value -0.09. **B.** Intermediate pattern shows correlation 0.49. **C.** Pattern with largest area of same value shows highest correlation 0.75.

MCF-7 estradiol (-) group can be explained by the diffuse multifocal pattern necrosis found in the MDA-MB-231 group. The higher vascularity (higher MVD), observed in the MDA-MB-231 group may prevent a confluent necrosis, leading to the preservation of linearity of neighboring pixel values of the ADC map. Based on our results, the second texture analysis of ADC maps can provide quantitative spatial information about the necrosis pattern as described by the vascularity.

The use of a 9.4-T animal MRI is another notable aspect of our study. The improvement of the signal to noise ratio through a subcutaneous tumor location and high-field strength is the main factor that enabled our texture analysis in tumor models (31). DW-MRI is an appealing imaging modality to examine tumor aggressiveness and responsiveness to therapy in the field of oncology because it can be easily incorporated into the clinical practice due to its non-invasiveness and quick acquisition time without contrast agents (32). Tumors with lower ADC values have been reported to correlate with higher cellularity, a tortuous extracellular space and a rapid tumor growth rate (33, 34). In an animal model, DW-MRI showed a higher sensitivity than T2-weighted MR images in the detection of colorectal liver metastasis (35). A recent study reported that the ADC values of epithelial-like xenograft tumors were lower than those of mesenchymal-like tumors (36). In the clinical MRI, a controversy remains regarding the relationship between mean ADC values and lesion aggressiveness characteristics, such as histologic grade, tumor size or axillary lymph node metastasis (37, 38). In our study, although we found that texture analysis parameters were different among the MCF-7 estradiol (+), MCF-7 estradiol (-), and MDA-MB-231 tumor groups; no significant difference was found in the mean ADC values. Therefore, we believe that the texture analysis of ADC maps obtained by high-strength MRI can provide more refined information about tumor cellularity or extracellular space reflecting cellular proliferation than the mean ADC analysis of the clinical MRI.

The quantification of intratumoral heterogeneity provides relevant information for making decisions during a specific treatment. The most aggressive clones within a tumor tend to survive, replicate and metastasize during the eradication of clones sensitive to treatment (39). A serial biopsy might be used for the metastatic lesions to detect the clonal evolution for a targeted therapy (2). However, considering sampling bias and practical applicability issues, non-invasive monitoring methods evaluating tumor cellularity and possible epithelial mesenchymal transition by reflecting water motion changes could be a promising alternative in future research (36).

There are several limitations in this study. First, we used a 9.4-T animal MR machine with a surface coil. Animal tumor models usually tend to grow more rapidly than human patient tumors and it is known that animal tumor models show less intra- and inter-tumoral heterogeneity (31). Thus, we cannot directly extrapolate our results to humans. In addition, the radiofrequency field inhomogeneity of the surface coil used in our study could have exaggerated the contrast of the images, although all tumors underwent MR images by using the same surface coil. Second, we used a mono-exponential model to acquire all b-factors. Although several studies have reported that that the bi-exponential

Korean Journal of Radiology
KJR

model is accurate for the calculation of ADC values without the influence of microperfusion (40, 41), the clinical application of the bi-exponential model is still controversial (42-44). Third, MR images were obtained in different intervals between tumor implantation and MR examinations among the three groups. As the growth rates of each tumor group were various, it was inevitable to obtain the MR image at various intervals to minimize volumetric differences.

In conclusion, the MCF-7 tumors supplemented with estradiol showed more heterogeneous DW-MRI texture parameters than either the MCF-7 tumors without estradiol supplement or the MDA-MB-231 tumors, which were characterized by a higher cellular proliferation and central necrosis patterns. The MDA-MB-231 tumors showed less heterogeneous DW-MRI texture parameters than the MCF-7 tumors due to a higher vascularity and diffuse multifocal necrosis patterns. The texture analysis of the ADC maps of breast cancer xenograft models provided a quantitative measurement of the intratumoral heterogeneity of necrosis patterns mediated from proliferative activity and vascularity. Thus, the texture analysis of the DW-MRI could potentially be used as a non-invasive imaging method for the monitoring of the intratumoral heterogeneity of cellularity following the therapy in breast cancer patients.

REFERENCES

1. Perou CM, Sørlie T, Eisen MB, van de Rijn M, Jeffrey SS, Rees CA, et al. Molecular portraits of human breast tumours. *Nature* 2000;406:747-752
2. Bedard PL, Hansen AR, Ratain MJ, Siu LL. Tumour heterogeneity in the clinic. *Nature* 2013;501:355-364
3. Koh DM, Collins DJ. Diffusion-weighted MRI in the body: applications and challenges in oncology. *AJR Am J Roentgenol* 2007;188:1622-1635
4. Choi BB, Kim SH, Kang BJ, Lee JH, Song BJ, Jeong SH, et al. Diffusion-weighted imaging and FDG PET/CT: predicting the prognoses with apparent diffusion coefficient values and maximum standardized uptake values in patients with invasive ductal carcinoma. *World J Surg Oncol* 2012;10:126
5. Costantini M, Belli P, Distefano D, Bufi E, Matteo MD, Rinaldi P, et al. Magnetic resonance imaging features in triple-negative breast cancer: comparison with luminal and HER2-overexpressing tumors. *Clin Breast Cancer* 2012;12:331-339
6. Guo Y, Cai YQ, Cai ZL, Gao YG, An NY, Ma L, et al. Differentiation of clinically benign and malignant breast lesions using diffusion-weighted imaging. *J Magn Reson Imaging* 2002;16:172-178
7. Jeh SK, Kim SH, Kim HS, Kang BJ, Jeong SH, Yim HW, et al. Correlation of the apparent diffusion coefficient value and dynamic magnetic resonance imaging findings with prognostic factors in invasive ductal carcinoma. *J Magn Reson Imaging* 2011;33:102-109
8. Kamitani T, Matsuo Y, Yabuuchi H, Fujita N, Nagao M, Jinnouchi M, et al. Correlations between apparent diffusion coefficient values and prognostic factors of breast cancer. *Magn Reson Med Sci* 2013;12:193-199
9. Park SH, Moon WK, Cho N, Song IC, Chang JM, Park IA, et al. Diffusion-weighted MR imaging: pretreatment prediction of response to neoadjuvant chemotherapy in patients with breast cancer. *Radiology* 2010;257:56-63
10. Jung DC, Lee HJ, Seo JW, Park SY, Lee SJ, Lee JH, et al. Diffusion-weighted imaging of a prostate cancer xenograft model seen on a 7 Tesla animal MR scanner: comparison of ADC values and pathologic findings. *Korean J Radiol* 2012;13:82-89
11. Stephen RM, Pagel MD, Brown K, Baker AF, Meuillet EJ, Gillies RJ. Monitoring the development of xenograft triple-negative breast cancer models using diffusion-weighted magnetic resonance imaging. *Exp Biol Med (Maywood)* 2012;237:1273-1280
12. Davnall F, Yip CS, Ljungqvist G, Selmi M, Ng F, Sanghera B, et al. Assessment of tumor heterogeneity: an emerging imaging tool for clinical practice? *Insights Imaging* 2012;3:573-589
13. Karahaliou A, Vassiou K, Arikidis NS, Skiadopoulos S, Kanavou T, Costaridou L. Assessing heterogeneity of lesion enhancement kinetics in dynamic contrast-enhanced MRI for breast cancer diagnosis. *Br J Radiol* 2010;83:296-309
14. Haralick RM, Shanmugam K, Dinstein IH. Textural features for image classification. *IEEE Transactions on Systems, Man and Cybernetics* 1973;SMC-3:610-621
15. Chen W, Giger ML, Li H, Bick U, Newstead GM. Volumetric texture analysis of breast lesions on contrast-enhanced magnetic resonance images. *Magn Reson Med* 2007;58:562-571
16. Eary JF, O'Sullivan F, O'Sullivan J, Conrad EU. Spatial heterogeneity in sarcoma 18F-FDG uptake as a predictor of patient outcome. *J Nucl Med* 2008;49:1973-1979
17. Gibbs P, Turnbull LW. Textural analysis of contrast-enhanced MR images of the breast. *Magn Reson Med* 2003;50:92-98
18. Henriksson E, Kjellen E, Wahlberg P, Ohlsson T, Wennerberg J, Brun E. 2-Deoxy-2-[18F] fluoro-D-glucose uptake and correlation to intratumoral heterogeneity. *Anticancer Res* 2007;27:2155-2159
19. Sinha S, Lucas-Quesada FA, DeBruhl ND, Sayre J, Farria D, Gorczyca DP, et al. Multifeature analysis of Gd-enhanced MR images of breast lesions. *J Magn Reson Imaging* 1997;7:1016-1026
20. Tixier F, Le Rest CC, Hatt M, Albarghach N, Pradier O, Metges JP, et al. Intratumor heterogeneity characterized by textural features on baseline 18F-FDG PET images predicts response to concomitant radiochemotherapy in esophageal cancer. *J Nucl Med* 2011;52:369-378
21. van Velden FH, Cheebsumon P, Yaqub M, Smit EF, Hoekstra

OS, Lammertsma AA, et al. Evaluation of a cumulative SUV-volume histogram method for parameterizing heterogeneous intratumoural FDG uptake in non-small cell lung cancer PET studies. *Eur J Nucl Med Mol Imaging* 2011;38:1636-1647
22. Yu H, Caldwell C, Mah K, Poon I, Balogh J, MacKenzie R, et al. Automated radiation targeting in head-and-neck cancer using region-based texture analysis of PET and CT images. *Int J Radiat Oncol Biol Phys* 2009;75:618-625
23. Stejskal EO, Tanner JE. Spin diffusion measurements: spin echoes in the presence of a time-dependent field gradient. *J Chem Phys* 1965;42:288-292
24. Albregtsen F. *Statistical texture measures computed from gray level coocurrence matrices*. Norway: Image Processing Laboratory Department of Informatics University of Oslo, 2008
25. Huuse EM, Moestue SA, Lindholm EM, Bathen TF, Nalwoga H, Krüger K, et al. In vivo MRI and histopathological assessment of tumor microenvironment in luminal-like and basal-like breast cancer xenografts. *J Magn Reson Imaging* 2012;35:1098-1107
26. Zhu Z, Edwards RJ, Boobis AR. Increased expression of histone proteins during estrogen-mediated cell proliferation. *Environ Health Perspect* 2009;117:928-934
27. Katzenellenbogen BS, Kendra KL, Norman MJ, Berthois Y. Proliferation, hormonal responsiveness, and estrogen receptor content of MCF-7 human breast cancer cells grown in the short-term and long-term absence of estrogens. *Cancer Res* 1987;47:4355-4360
28. Downey K, Riches SF, Morgan VA, Giles SL, Attygalle AD, Ind TE, et al. Relationship between imaging biomarkers of stage I cervical cancer and poor-prognosis histologic features: quantitative histogram analysis of diffusion-weighted MR images. *AJR Am J Roentgenol* 2013;200:314-320
29. Kyriazi S, Collins DJ, Messiou C, Pennert K, Davidson RL, Giles SL, et al. Metastatic ovarian and primary peritoneal cancer: assessing chemotherapy response with diffusion-weighted MR imaging--value of histogram analysis of apparent diffusion coefficients. *Radiology* 2011;261:182-192
30. Nelson DA, Tan TT, Rabson AB, Anderson D, Degenhardt K, White E. Hypoxia and defective apoptosis drive genomic instability and tumorigenesis. *Genes Dev* 2004;18:2095-2107
31. Bokacheva L, Ackerstaff E, LeKaye HC, Zakian K, Koutcher JA. High-field small animal magnetic resonance oncology studies. *Phys Med Biol* 2014;59:R65-R127
32. Padhani AR, Liu G, Koh DM, Chenevert TL, Thoeny HC, Takahara T, et al. Diffusion-weighted magnetic resonance imaging as a cancer biomarker: consensus and recommendations. *Neoplasia* 2009;11:102-125
33. Barrett T, Gill AB, Kataoka MY, Priest AN, Joubert I, McLean MA, et al. DCE and DW MRI in monitoring response to androgen deprivation therapy in patients with prostate cancer: a feasibility study. *Magn Reson Med* 2012;67:778-785
34. Vossen JA, Buijs M, Geschwind JF, Liapi E, Prieto Ventura V, Lee KH, et al. Diffusion-weighted and Gd-EOB-DTPA-contrast-enhanced magnetic resonance imaging for characterization of tumor necrosis in an animal model. *J Comput Assist Tomogr* 2009;33:626-630
35. Wagner M, Maggiori L, Ronot M, Paradis V, Vilgrain V, Panis Y, et al. Diffusion-weighted and T2-weighted MR imaging for colorectal liver metastases detection in a rat model at 7 T: a comparative study using histological examination as reference. *Eur Radiol* 2013;23:2156-2164
36. Chen YW, Pan HB, Tseng HH, Chu HC, Hung YT, Yen YC, et al. Differentiated epithelial- and mesenchymal-like phenotypes in subcutaneous mouse xenografts using diffusion weighted-magnetic resonance imaging. *Int J Mol Sci* 2013;14:21943-21959
37. Kim SH, Cha ES, Kim HS, Kang BJ, Choi JJ, Jung JH, et al. Diffusion-weighted imaging of breast cancer: correlation of the apparent diffusion coefficient value with prognostic factors. *J Magn Reson Imaging* 2009;30:615-620
38. Razek AA, Gaballa G, Denewer A, Nada N. Invasive ductal carcinoma: correlation of apparent diffusion coefficient value with pathological prognostic factors. *NMR Biomed* 2010;23:619-623
39. Nowell PC. The clonal evolution of tumor cell populations. *Science* 1976;194:23-28
40. Le Bihan D, Breton E, Lallemand D, Grenier P, Cabanis E, Laval-Jeantet M. MR imaging of intravoxel incoherent motions: application to diffusion and perfusion in neurologic disorders. *Radiology* 1986;161:401-407
41. Liu C, Liang C, Liu Z, Zhang S, Huang B. Intravoxel incoherent motion (IVIM) in evaluation of breast lesions: comparison with conventional DWI. *Eur J Radiol* 2013;82:e782-e789
42. Doblas S, Wagner M, Leitao HS, Daire JL, Sinkus R, Vilgrain V, et al. Determination of malignancy and characterization of hepatic tumor type with diffusion-weighted magnetic resonance imaging: comparison of apparent diffusion coefficient and intravoxel incoherent motion-derived measurements. *Invest Radiol* 2013;48:722-728
43. Sigmund EE, Cho GY, Kim S, Finn M, Moccaldi M, Jensen JH, et al. Intravoxel incoherent motion imaging of tumor microenvironment in locally advanced breast cancer. *Magn Reson Med* 2011;65:1437-1447
44. Tamura T, Usui S, Murakami S, Arihiro K, Akiyama Y, Naito K, et al. Biexponential Signal Attenuation Analysis of Diffusion-weighted Imaging of Breast. *Magn Reson Med Sci* 2010;9:195-207